Extending the Applicability of Exact Nuclear Overhauser Enhancements to Large Proteins and RNA

Parker J. Nichols,[a] Alexandra Born,[a] Morkos A. Henen,[a, b] Dean Strotz,[c] Chi N. Celestine,[d] Peter Güntert,[c, e, f] and Beat Vögeli*[a]

Distance-dependent nuclear Overhauser enhancements (NOEs) are one of the most popular and important experimental restraints for calculating NMR structures. Despite this, they are mostly employed as semiquantitative upper distance bounds, and this discards the wealth of information that is encoded in the cross-relaxation rate constant. Information that is lost includes exact distances between protons and dynamics that occur on the sub-millisecond timescale. Our recently introduced exact measurement of the NOE (eNOE) requires little additional experimental effort relative to other NMR observables. So far, we have used eNOEs to calculate multistate ensembles of proteins up to approximately 150 residues. Here, we briefly revisit eNOE methodology and present two new directions for the use of eNOEs: applications to large proteins and RNA.

1. Introduction

Since the first X-ray structures of myoglobin and the DNA double helix were first determined and proposed in 1958 and 1953, respectively, accurate determination of the 3D structures of biomolecules has been a cornerstone in molecular biology and biochemical research. Whereas single-state averaged structures and simple lock-and-key models have been the most prominent paradigms for the majority of the 20th century, our current view of biomolecules realizes the importance of dynamics for their functions. In proteins, increasing evidence shows the importance of concerted motions and allosteric responses in enzymatic reactions,[1–4] protein–ligand interactions,[5–8] adaptive responses,[1,2,4] and the protein folding process. Intrinsically disordered proteins are capable of adopting many different conformations to form ternary complexes with a variety of binding partners.[3] In parallel, it is recognized that conformational changes and other important functions of RNA rely on dynamic motions that occur on the timescale of picoseconds to seconds.[9] These include secondary-structure transitions that modulate RNA–ligand binding sites in response to ligand concentration and temperature,[10–13] as well as base-pair melting, reshuffling, and isomerization that regulate RNA–protein and RNA–RNA interactions[14–22] and catalysis in the ribosome and spliceosome.[23–27] These types of motions can be coupled to each other to result in an overall tertiary structure rearrangement.[28] Additionally, RNA interhelical and loop dynamics have been shown to be critical for many RNA recognition processes.[29–33] Thus, a full understanding of how such biomolecules function requires not only accurate 3D models but also a comprehensive description of their dynamics.

NMR spectroscopy is well suited to tackle such requirements. Whereas spin-relaxation methods can be used to characterize single-site flexibility and exchange,[34] NMR observables such as nuclear Overhauser enhancements (NOEs), scalar couplings, and residual dipolar couplings (RDCs), which report on internuclear distances, torsion angles, and internuclear vector orientations, respectively, can be used to determine the tertiary and global structure.[35–39] Whereas the application of NMR spectroscopy to larger biomolecules is fundamentally limited by fast transverse relaxation rates (R_2) and signal overlap, significant advances have been made that allow for measurements of NMR observables in systems of increasingly larger molecular weight. Examples include transverse relaxation-optimized spectroscopy (TROSY) and cross-correlated relaxation-enhanced polarization transfer (CRINEPT) sequences,[40–44] as well as perdeuteration, possibly in combination with selective methyl reprotonation,[45–49] which have enabled binding studies for a number of supramolecular protein complexes that are greater than 200 kDa.[50–56] The size of RNA structures that can be investigated by NMR spectroscopy has also been signifi-

[a] P. J. Nichols, A. Born, Prof. Dr. M. A. Henen, Prof. Dr. B. Vögeli
Department of Biochemistry and Molecular Genetics
University of Colorado Denver, Anschutz Medical Campus
12801 East 17th Avenue, Aurora, CO 80045 (USA)
E-mail: beat.vogeli@ucdenver.edu

[b] Prof. Dr. M. A. Henen
Faculty of Pharmacy, Mansoura University
Mansoura 35516 (Egypt)

[c] Dr. D. Strotz, Prof. Dr. P. Güntert
Laboratory of Physical Chemistry, ETH Zürich
Vladimir-Prelog-Weg 2, 8093 Zürich (Switzerland)

[d] Dr. C. N. Celestine
Department of Medical Biochemistry and Microbiology
Uppsala University
BMC Box 582, 75123 Uppsala (Sweden)

[e] Prof. Dr. P. Güntert
Institute of Biophysical Chemistry, Goethe Universität Frankfurt
Max-von-Laue-Strasse 9, 60438 Frankfurt am Main (Germany)

[f] Prof. Dr. P. Güntert
Graduate School of Science, Tokyo Metropolitan University
1-1 Minami-ohsawa, Hachioji, Tokyo 192-0397 (Japan)

[ID] The ORCID identification numbers for the authors of this article can be found under https://doi.org/10.1002/cbic.201800237.

cantly increased by the implementation of isotope-labeling strategies,[57–59] "divide-and-conquer" and "cut-and-paste" methods,[60,61] solid-state NMR spectroscopy techniques,[62] and protocols that incorporate a diverse range of structural and biochemical data.[63] Such advances have pushed NMR spectroscopy to heights that were originally thought impossible.

With such inspiring advances, it can be easy to forget about one of the most long-standing and informative NMR observables, the nuclear Overhauser enhancement. Conventional NOEs are mostly employed as semiquantitative upper distance restraint limits, or in the case of the before-mentioned supramolecular complexes, as a tool to confirm assignments of methyl groups.[64,65] Although useful, there is significant room for improvement. We previously reported on the theory and use of exact nuclear Overhauser enhancements (eNOEs) for the determination of distances in Ubiquitin and GB3 of up to 5 Å with only 0.1 Å error.[66,67] The unprecedented accuracy of eNOEs allows for high-resolution structures to be calculated from eNOEs alone.[68,69] In cases for which dense eNOE networks can be acquired, multistate structure calculations can be performed that capture spatial fluctuations that would otherwise be missed by conventional NOEs.[68,70,71] In addition, we showed that eNOEs contain similar and complementary information to both J couplings and RDCs.[72] So far, we have only used eNOEs to calculate multistate ensembles of proteins up to about 150 resides.[73,74] Currently, we are testing new directions for the applications of eNOE methodology.

Exploiting the exceptional accuracy of eNOEs, we investigated their usefulness as a tool to determine distances within supramolecular complexes and to help define RNA molecules for which a lack of chemical-shift diversity and NOE density makes defining structures problematic.[75] To this end, we recently applied our eNOE protocol to determine inter-methyl distances in the 360 kDa proteasome[76] as well as the 14-mer UUCG RNA tetraloop.[77] Here, we briefly review the eNOE protocol and then discuss these most recent advances.

1.1. What is the difference between NOEs and eNOEs?

Although the NOE rate constant is proportional to the inverse sixth power of the distance between two dipolar interacting spins (r^{-6}),[78] NOEs are mostly employed as semiquantitative upper distance limit restraints instead of exact averaged values.[39] This practice has resulted from the difficulty in converting NOEs into exact distances for large biomolecules.[79] Specifically, extracting accurate NOE cross-relaxation rate constants (σ) is hampered by interfering mechanisms throughout the pulse sequence[80] but mainly by spin diffusion that is relayed by neighboring spins.[79,81] We introduced a formalism that is able to correct for these issues,[82] allowing for the conversion of σ rates into an almost exact distance between the two atoms in question (exact NOEs or eNOEs). The formalism is complex and was thoroughly described previously,[82,83] so we will not review it here.

2. Step-by-Step Guide for Extracting eNOEs

2.1. Acquiring a NOESY buildup series

We developed an easy-to-implement protocol for the extraction of eNOEs from any system of interest. The first step of the protocol is to measure either a 2D or 3D NOESY buildup series (Figure 1, step 1). For the 3D case, we usually use a NOESY HSQC pulse sequence with simultaneous evolution of ^{15}N and ^{13}C[83] (for application to large systems, we recommend 3D HMQC NOESY HMQC, see Section 3.1.). Theoretically, only two mixing times are required; however, to achieve high-quality fits of the data and to improve accuracy, we recommend at least four. All mixing time points within the series must be measured during the same measurement session, and we recommend that the order be randomized in the case of time-dependent sample changes. Assuming an inverse relationship between the maximal mixing time and the overall rotational correlation time (τ_c), we derived theoretical optimal upper limit mixing times of approximately 2.5×10^{-10} and 4×10^{-10} $s^2 \tau_c^{-1}$ for proteins and RNA, respectively.[77,82] NOESY mixing periods beyond these values will incur relatively large errors in the extracted σ values owing to increasing spin diffusion; however, longer mixing times are used for assignment purposes. After acquiring the buildup series, we assign the signals in the spectra from the longest NOESY mixing time and exclude overlapped diagonal and crosspeaks, although cross-peak buildups with overlapped diagonals can still be used in the form of generically normalized eNOEs (gn-eNOEs),[84] as described later. The intensities for the cross and diagonal peaks are then extracted for the entire series of mixing times by using the nlinLS script within NMRPipe[85] or a similar script of choice.

2.2. Fitting the buildups

The intensities from the cross and diagonal peaks are then fitted to monoexponential buildup and decay curves by using the eNORA2[86] package, which has been implemented into the most recent version of CYANA[87,88] (note that the stand-alone eNORA2 package coded in MATLAB is available for download but cannot handle RNA molecules). eNORA2 fits diagonal peak decays as a function of the mixing time to determine both the autorelaxation rate constant (ρ) as well as the initial magnetization at zero mixing time [$\Delta M(0)$]. In parallel, spin-diffusion corrections are calculated from a previously determined NMR ensemble or X-ray structure and applied to the intensities of the cross-peak buildup curves. Note that if no structure is available, a preliminary structure by using conventional NOEs will need to be calculated first. This structure may then be used as an input for spin-diffusion treatment in eNOE distance determination.

There are two methods that can be used to calculate spin diffusion: the full-matrix approach and the three-spin approach.[82,89] For most applications, the full-matrix approach is superior, because the magnetization transfer pathways between all spins are considered simultaneously. The three-spin
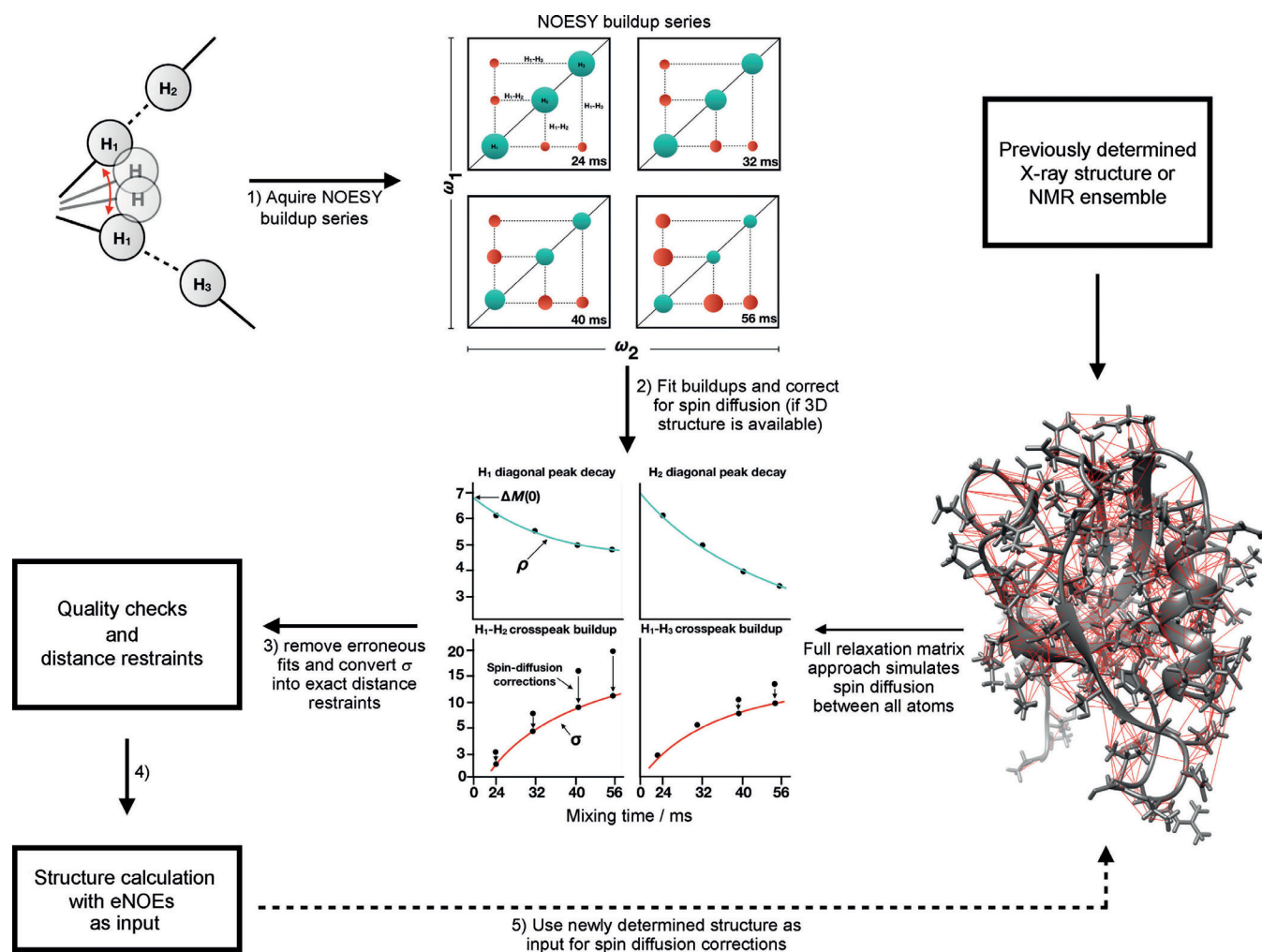
Figure 1. The eNOE protocol. The cross-relaxation rate (σ) between two dipolar interacting spins increases as a function of the mixing time (τ_{mix}) and is proportional to r^{-6} (step 1). Acquiring a NOESY buildup series allows for the autorelaxation rates (ρ) and initial magnetizations [$\Delta M(0)$] to be fitted (step 2). These can then be used in combination with spin-diffusion corrections to fit accurate σ rates (step 2). Once erroneous fits are removed by visual inspection of the plotted ρ and σ rates, σ can be converted into exact internuclear distances through its proportionality to r^{-6} (step 3). After adding a user-defined error to the effective distances derived from unidirectional and generically normalized eNOEs, the eNOE distance restraints can be used as input for structure calculations (step 4). We recommend an error of 20% for proteins and 10% for RNA; however, the applied error is case dependent. If the input structure for spin-diffusion calculations is not of exceptional quality, the newly acquired eNOE structure can be used as the input for spin-diffusion corrections in an iterative process (step 5). In cases for which robust eNOE networks can be acquired, multistate structure calculations can be performed in CYANA.

approach is well-suited for partially deuterated biomolecules.[89]

eNORA2 will then proceed to fit the σ values by using the corrected cross-peak buildup intensities and the fitted ρ and $\Delta M(0)$ values (Figure 1, step 2). The corrected σ rates are then converted into bidirectional (both symmetry-related crosspeaks can be normalized to their corresponding diagonal peaks) and unidirectional (only one crosspeak can be evaluated or the eNOE cannot be normalized to both diagonal peaks) eNOE effective distance restraints through the relationship $\sigma \propto r^{-6}$. Note that both the spin diffusion corrections and conversion of σ into effective distances require a relatively accurate value for the overall rotational correlation time (τ_c) as input.

Effective distances from unidirectional eNOEs should be given a user-defined error (we recommend 20 and 10% for proteins and RNA, respectively), whereas bidirectional eNOEs require no tolerance adjustment and will have the same dis-

tance for both the upper and lower distance limits. eNORA2 and CYANA will only calculate unidirectional eNOEs if the crosspeak can be normalized to its corresponding diagonal peak. Because there are two alternative pathways of magnetization transfer (from spin $i \rightarrow j$ and from spin $j \rightarrow i$), there will be effective distances missing from each choice of pathway that may be present in the other. Depending on the choice of the NOESY experiment,[80] normalization to the peak intensity of the spin of origin ($i \rightarrow j$) or destination ($j \rightarrow i$) is more theoretically sound. For example, if a HSQC element is used after the NOESY transfer, the different relaxation rates of spins i and j during the HSQC may result in stronger differentiation of the intensities than the one caused by nonuniform equilibrium re-establishment before NOESY mixing. Nevertheless, we also always add unidirectional eNOEs that are exclusive to the other normalization to our list to increase the total amount of eNOEs.

For the extraction of gn-eNOEs from overlapped diagonals, it is necessary to determine the average ρ value as well as an upper limit $\Delta M(0)$ on the basis of the nonoverlapped values in the output lists. It is recommended to distinguish single, methylene, and methyl protons upon choosing average ρ values and upper limit $\Delta M(0)$ values that are safely above all fitted $\Delta M(0)$ values. An improved method is to use averaged ρ and upper limit $\Delta M(0)$ values for each specific atom type. eNORA2 can then use these values to calculate gn-eNOEs from cross-peak buildups associated with overlapped diagonals, which can be used as upper limit restraints in conjunction with the bidirectional and unidirectional eNOE restraints. gn-eNOEs should be given the same upper limit error as unidirectional eNOEs.

2.3. eNOE structure calculation

Once the eNOEs are calculated, we visually inspect the buildup plots and remove poor fits (Figure 1, step 3). Calculating an eNOE structure simply requires the use of the eNOE and gn-eNOE distance restraints as input for a conventional structure calculation (Figure 1, step 4). Note that the calculated structure can then be used as the input for spin-diffusion calculations, which allows for an iterative process (Figure 1, step 5).

For dense eNOE networks (an exceptional case is shown in Figure 1), multistate structures can be calculated in CYANA that allow visualization of spatial sampling. This is due to the averaged nature of eNOEs,[73] and consequently, an atom that samples multiple points in space will produce eNOE distances to nearby atoms that are the r^{-6} averages of all the distances sampled. If a sufficient amount of eNOEs define such an atom, then the combined network contains information about all of the sampled substates. Thus, single-state structure calculations will result in many violated distance restraints, because the eNOEs cannot be fulfilled simultaneously by a single structure. Multiple states allow for such violated eNOE restraints to be satisfied, which captures the spatial sampling of the biomolecule in the process.

3. eNOE Recent Applications

3.1. eNOEs in a 360 kDa proteasome complex

We recently measured eNOEs in the 360 kDa 2×7-mer half proteasome from *Thermoplasma acidophilium*.[76] For proteins larger than about 150 residues, diagonal peak overlap becomes a limiting factor for the extraction of usable eNOEs.[84] In addition, our simulations for molecules with a rotational correlation time of 150 ns or larger showed that the spin diffusion between neighboring methyl groups within the same valine or leucine side chain could be an order of magnitude larger than the direct NOE transfer. This made it impossible to perform accurate spin-diffusion corrections so that quantitative distances could be obtained.[89] Therefore, we measured eNOEs on a sample that was perdeuterated and selectively methyl labeled at the Ileδ1, Valγ2, and Leuδ2 positions (Figure 2A). Spin-diffusion corrections calculated by using the full-matrix approach for this labeling scheme were possible, and this allowed for a NOESY buildup series to be measured for $\tau_{mix} = 30$, 60, 90, and

120 ms. We were able to extract 18 bidirectional eNOEs, an additional 14 unidirectional eNOEs if normalized to the spin of origin, and 29 unidirectional eNOEs if normalized to the spin of destination (Figure 2A). We compared the extracted bi- and unidirectional eNOE distances to two high-resolution X-ray structures of the proteasome: one in the free form determined at 3.4 Å resolution (PDB ID: 1PMA)[90] and the other bound to the 11S activator determined at 1.9 Å resolution (PDB ID: 1YA7).[91] Pearson's correlation coefficients for only bi-directional and bi- or unidirectional eNOE distances compared to distances from 1PMA were 0.80 and 0.64, respectively. If compared to 1YA7, they were 0.89 and 0.78, respectively, thus indicating that 1YA7 better represents the liquid-state conformation (Figure 2B). In addition, we found a number of eNOE distances that were more than 1 Å shorter (Figure 2C, blue) or longer (Figure 2C, red) than the corresponding distances from 1YA7. Strikingly, almost all of these violated distance restraints correlated to residues with order parameters smaller than 0.33,
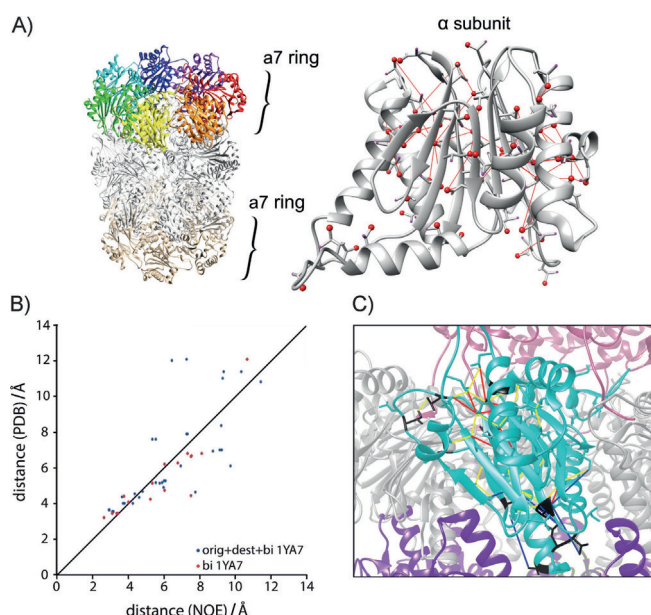
Figure 2. eNOEs in the 360 kDa proteasome. A) Left: ribbon backbone plot of the entire PDB ID 1PMA consisting of two heptameric α rings (colored) and two heptameric β rings (white). Right: the side chains of Val, Leu, and Ile are plotted on the ribbon backbone of an individual α subunit. The NOE-sensitive ¹H,¹³C-labeled methyl groups (Ileδ1, Valγ2, and Leuδ2) are highlighted by red spheres at the carbon positions. Methyl pairs for which build-ups could be measured are connected by red lines. B) Distances extracted from the X-ray structure 1YA7 on the *x*-axis versus those from eNOEs on the *y*-axis. The intensities of the crosspeaks of unidirectional eNOEs were normalized with diagonal peak intensities of magnetization of origin or destination. eNOEs were extracted from a NOESY buildup series with mixing times of 30, 60, 90, and 120 ms. Corrections for spin diffusion were estimated with the full-relaxation matrix approach, and the resulting distances were scaled by 1.09 to account for incomplete deuteration (as determined from the three-spin approach). An overall τ_c of 148 ns was extrapolated from ref. [64] Theoretical distances were extracted with r^{-6} averaging from the 1YA7 PDB structure. C) Clustering of deviations of experimental from X-ray distances. Distances that are at least 1 Å larger or smaller than those extracted from the X-ray structure 1YA7 are shown in red and blue, respectively, and those within 1 Å are shown in yellow. The distances are plotted on the α subunit A (cyan), and other α subunits in the same ring are shown in white. Residues with methyl axis order parameters smaller than 0.33 are colored black. 11S activator and the β ring are shown in pink and purple, respectively.
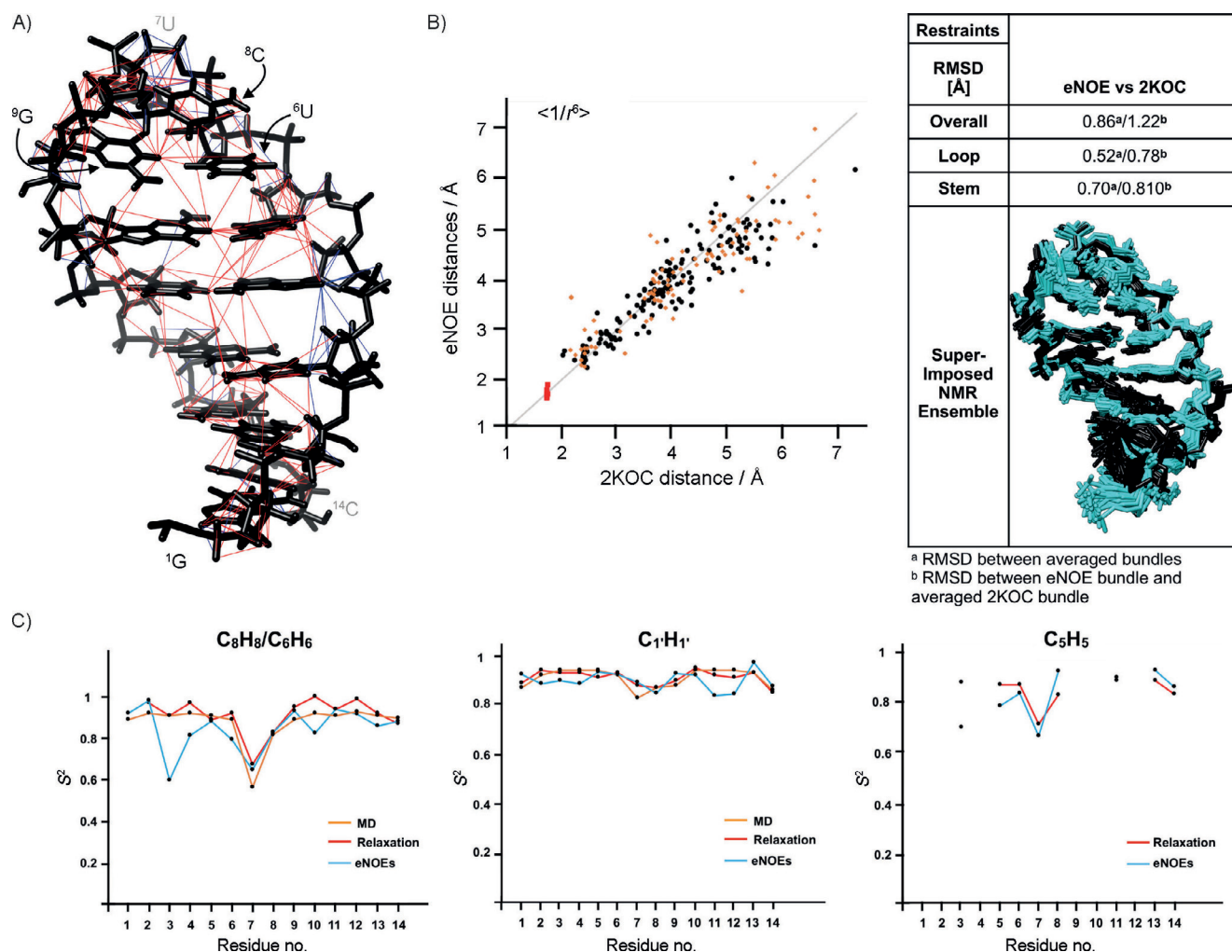
Figure 3. Defining the 14mer UUCG tetraloop by using eNOEs. A) The 265 extracted eNOEs (red) and 88 gn-eNOEs (blue) are plotted onto the NMR structure 2KOC. B-Left) Correlation plot between distances from 2KOC on the x axis and eNOE effective distances from fits of 40–160 ms on the y axis (overall correlation: $y = 0.96x$, $R = 0.89$). Black circles correspond to distances between non-amino/non-methylene protons ($y = 0.96x$, $R = 0.89$), orange diamonds correspond to distances between amino/methylene protons and non-amino/non-methylene or amino/methylene protons on a different residue ($y = 0.96x$, $R = 0.84$), and red squares correspond to distances within amino/methylene spin pairs ($y = 0.98x$, $R = 0.35$). B-Right) Superposition of the eNOE structure (black) and 2KOC (cyan). Reported RMSD values are for heavy atoms. C) Comparison of order parameters S^2 backcalculated from the two-state eNOE ensemble and experimentally and computationally derived S^2 values. eNOE S^2 are shown in blue, NMR relaxation S^2 in red, and molecular dynamics S^2 in orange.

as determined by Kay and co-workers (Figure 2 C, black lines).[64,92] In addition, two clusters with systematic differences emerged. The eNOE distances that were longer in the X-ray structure were found to involve residues that anchored loop 201–210, which in turn formed the interface with the 11S activator (shown in pink). Under our experimental conditions, this loop was solvent exposed, which may explain the more extended nature of the distance network. Indeed, the distances from 1PMA were longer, although the eNOE distances were still larger. The cluster that contained distances that were shorter than those in the X-ray structure involved the segment that interacted with the β ring. Under our experimental conditions, this segment was instead in complex with the second α ring, thus indicating that the structural differences at the interface are dependent upon the interacting subunit. These findings highlight the potential ability of eNOEs to pinpoint changes in molecular structure upon rearrangements such as binding events and allosteric motions.

This study was significant because it was one of the first for which internuclear distances were extracted from supramolecular complexes. Without spin-diffusion corrections, the extracted distances would not even be sufficient for a simple three-class interpretation. Although we noted that the extracted distances were less accurate than those extracted for small proteins, the distances still correlated well with the high-resolution X-ray structures. The quality of the structure used to calculate the spin-diffusion corrections is also important. Given the signal-to-noise ratio in our spectra, it is clear that such measurements are feasible for molecules with molecular weights up to 1 MDa and even beyond.

3.2. High-resolution RNA structures from eNOEs

Another recent use of eNOEs was to define the structure of a 14-mer RNA UUCG tetraloop.[77] RNA only contains 4 chemically unique building blocks, as opposed to 20 for proteins, and

consequently, the NMR spectrum of RNA suffers from significant spectral overlap.[75] This problem is further exacerbated by the predominately A-form helical structure of RNA molecules, which results in a lack of chemical-shift diversity. Additionally, RNA has a lower proton density than proteins, and thus, the number of NOEs that can be extracted is significantly smaller. As such, 3D RNA structures of RNA can rarely reach high resolution from NOEs alone[75,93] and often require time-consuming measurements of additional NMR observables such as dihedral angle restraints, RDCs,[94] cross-correlated relaxation rates,[95–97] paramagnetic resonance measurements,[98] and hydrogen-bonding patterns. Therefore, we investigated the usefulness of eNOEs in defining RNA molecules.

We measured a 2D NOESY buildup series with $\tau_{mix} = 40$, 80, 120, 160, 200, 240, 280, and 320 ms, although we only fitted eNOEs up to 160 ms because our simulations showed that effective distance errors from spin diffusion up to this time were below 2%. After excluding erroneous fits, we were able to extract a total of 265 eNOEs and 88 gn-eNOEs (Figure 3 A). The extracted effective distances correlated quite well to those from the high-resolution NMR structure (PDB ID: 2KOC;[93] Figure 3 B, left, $R = 0.89$). Our calculated structure ensemble with no restraint input other than eNOEs and gn-eNOEs had an overall heavy atom root-mean-square deviation (RMSD) of 0.44 Å, with a RMSD of 0.23 Å within the c(UUCG)g loop itself. We also compared our eNOE structure to 2KOC by calculating RMSD values between averaged bundles and between the full eNOE bundle and the averaged 2KOC structure (Figure 3 B, right). The agreement with 2KOC was significantly better for our eNOE structure than for a conventional structure calculated by using 677 semiquantitative NOEs (averaged and bundle-to-averaged RMSD values of 0.86 and 1.22 Å compared to 1.22 and 2.49 Å, respectively). Despite the eNOEs being able to define the 14-mer structure to 0.44 Å, the CYANA target function was relatively high, which indicated that many of the eNOE restraints were violated. Therefore, we calculated a two-state eNOE ensemble that revealed minor base-pair dynamics and correlated motions within the c(UUCG)g tetraloop itself. In addition, we backcalculated order parameters from our two-state ensemble that agreed well with previously determined S^2 values from relaxation rate measurements[99–102] (Figure 3 C).

These results indicate that the exact nature of the eNOEs allows for accurate single-state structure calculations and for spatial sampling to be probed in favorable cases for which many eNOEs can be acquired. Owing to the experimental ease of measuring a NOESY buildup series, this provides a new NMR spectroscopy method for investigating RNA structure and function.

4. Conclusions

We reviewed our exact measurement of the nuclear Overhauser enhancement (eNOE) protocol and presented its most recent applications to biological systems. We have shown that eNOEs could be used to extract fairly accurate distances from supramolecular complexes and could be a useful tool in binding studies and probing dynamics in such cases. eNOEs alone

could be used to define RNA structures to high resolution and, in favorable cases, to investigate spatial sampling. Experimentally, eNOEs were readily available. The only requirement was the measurement of three more NOESYs than what would normally be acquired. It is our hope that eNOEs will help the NMR spectroscopy community in their investigations of biological systems.

Conflict of Interest

The authors declare no conflict of interest.

[1] T. H. Kim, P. Mehrabi, Z. Ren, A. Sljoka, C. Ing, A. Bezginov, L. Ye, R. Pomès, R. S. Prosser, E. F. Pai, *Science* **2017**, *355*, eaag2355.
[2] D. A. Capdevila, J. J. Braymer, K. A. Edmonds, H. Wu, D. P. Giedroc, *Proc. Natl. Acad. Sci. USA* **2017**, *114*, 4424–4429.
[3] R. B. Berlow, H. J. Dyson, P. E. Wright, *Nature* **2017**, *543*, 447–451.
[4] E. Papaleo, G. Saladino, M. Lambrughi, K. Lindorff-Larsen, F. L. Gervasio, R. Nussinov, *Chem. Rev.* **2016**, *116*, 6391–6423.
[5] H. van den Bedem, J. S. Fraser, *Nat. Methods* **2015**, *12*, 307–318.
[6] T. R. M. Barends, L. Foucar, A. Ardevol, K. Nass, A. Aquila, S. Botha, R. B. Doak, K. Falahati, E. Hartmann, M. Hilpert, M. C. Hoffmann, J. Köfinger, J. E. Koglin, G. Kovacsova, M. Liang, D. Milathianaki, H. T. Lemke, J. Reinstein, C. M. Roome, R. L. Shoeman, G. J. Williams, I. Burghardt, G. Hummer, S. Boutet, I. Schlichting, *Science* **2015**, *350*, 445–450.
[7] D. R. Hekstra, K. I. White, M. A. Socolich, R. W. Henning, V. Šrajer, R. Ranganathan, *Nature* **2016**, *540*, 400–405.
[8] C. N. Chi, A. Bach, Å. Engström, H. Wang, K. Strømgaard, S. Gianni, P. Jemth, *Biochemistry* **2009**, *48*, 7089–7097.
[9] A. M. Mustoe, C. L. Brooks, H. M. Al-Hashimi, *Annu. Rev. Biochem.* **2014**, *83*, 441–466.
[10] W. Winkler, A. Nahvi, R. R. Breaker, *Nature* **2002**, *419*, 952–956.
[11] R. R. Breaker, *Cold Spring Harbor Perspect. Biol.* **2012**, *4*, a003566.
[12] A. Haller, M. F. Soulière, R. Micura, *Acc. Chem. Res.* **2011**, *44*, 1339–1348.
[13] J. Kortmann, S. Sczodrok, J. Rinnenthal, H. Schwalbe, F. Narberhaus, *Nucleic Acids Res.* **2011**, *39*, 2855–2868.
[14] S. A. Woodson, *RNA Biol.* **2010**, *7*, 677–686.
[15] E. Jankowsky, *Trends Biochem. Sci.* **2011**, *36*, 19–29.
[16] N. Shankar, T. Xia, S. D. Kennedy, T. R. Krugh, D. H. Mathews, D. H. Turner, *Biochemistry* **2007**, *46*, 12665–12678.
[17] G. L. Conn, D. E. Draper, E. E. Lattman, A. G. Gittis, *Science* **1999**, *284*, 1171–1174.
[18] Y. X. Wang, S. Huang, D. E. Draper, *Nucleic Acids Res.* **1996**, *24*, 2666–2672.
[19] A. M. Mustoe, M. H. Bailor, R. M. Teixeira, C. L. Brooks, H. M. Al-Hashimi, *Nucleic Acids Res.* **2012**, *40*, 892–904.
[20] E. A. Dethoff, K. Petzold, J. Chugh, A. Casiano-Negroni, H. M. Al-Hashimi, *Nature* **2012**, *491*, 724–728.
[21] K. T. Schroeder, D. M. J. Lilley, *Nucleic Acids Res.* **2009**, *37*, 7281–7289.
[22] B. M. Znosko, S. D. Kennedy, P. C. Wille, T. R. Krugh, D. H. Turner, *Biochemistry* **2004**, *43*, 15822–15837.
[23] C. G. Hoogstraten, J. R. Wank, A. Pardi, *Biochemistry* **2000**, *39*, 9951–9958.
[24] R. Yajima, D. J. Proctor, R. Kierzek, E. Kierzek, P. C. Bevilacqua, *Chem. Biol.* **2007**, *14*, 23–30.
[25] B. M. Kadakkuzha, L. Zhao, T. Xia, *Biochemistry* **2009**, *48*, 3807–3809.
[26] V. Venditti, L. Clos, N. Niccolai, S. E. Butcher, *J. Mol. Biol.* **2009**, *391*, 894–905.
[27] N. J. Reiter, H. Blad, F. Abildgaard, S. E. Butcher, *Biochemistry* **2004**, *43*, 13739–13747.
[28] M. Wu, I. Tinoco, *Proc. Natl. Acad. Sci. USA* **1998**, *95*, 11555–11560.

[29] R. W. Alexander, J. Eargle, Z. Luthey-Schulten, *FEBS Lett.* **2010**, *584*, 376–386.

[30] B. Heppell, S. Blouin, A. M. Dussault, J. Mulhbacher, E. Ennifar, J. C. Penedo, D. A. Lafontaine, *Nat. Chem. Biol.* **2011**, *7*, 384–392.

[31] N. Leulliot, G. Varani, *Biochemistry* **2001**, *40*, 7947–7956.

[32] T. Xia, *Curr. Opin. Chem. Biol.* **2008**, *12*, 604–611.

[33] T. Hermann, D. J. Patel, *Science* **2000**, *287*, 820–825.

[34] Y. Xue, J. M. Ward, T. Yuwen, I. S. Podkorytov, N. R. Skrynnikov, *J. Am. Chem. Soc.* **2012**, *134*, 2555–2562.

[35] N. Tjandra, A. Bax, *Science* **1997**, *278*, 1111–1114.

[36] A. Bax, *Protein Sci.* **2003**, *12*, 1–16.

[37] J. R. Bothe, E. N. Nikolova, C. D. Eichhorn, J. Chugh, A. L. Hansen, H. M. Al-Hashimi, *Nat. Methods* **2011**, *8*, 919–931.

[38] B. S. Tolbert, Y. Miyazaki, S. Barton, B. Kinde, P. Starck, R. Singh, A. Bax, D. A. Case, M. F. Summers, *J. Biomol. NMR* **2010**, *47*, 205–219.

[39] K. Wüthrich, *NMR of Proteins, Nucleic Acids*, Wiley, Hoboken, **1986**.

[40] K. Pervushin, R. Riek, G. Wider, K. Wüthrich, *Proc. Natl. Acad. Sci. USA* **1997**, *94*, 12366–12371.

[41] R. Riek, G. Wider, K. Pervushin, K. Wüthrich, *Proc. Natl. Acad. Sci. USA* **1999**, *96*, 4918–4923.

[42] G. Wider, K. Wüthrich, *Curr. Opin. Struct. Biol.* **1999**, *9*, 594–601.

[43] R. Riek, K. Pervushin, K. Wüthrich, *Trends Biochem. Sci.* **2000**, *25*, 462–468.

[44] A. Eletsky, S. V. S. R. K. Pulavarti, V. Beaumont, P. Gollnick, T. Szyperski, *J. Am. Chem. Soc.* **2015**, *137*, 11242–11245.

[45] N. K. Goto, L. E. Kay, *Curr. Opin. Struct. Biol.* **2000**, *10*, 585–592.

[46] K. H. Gardner, L. E. Kay, *Annu. Rev. Biophys. Biomol. Struct.* **1998**, *27*, 357–406.

[47] B. T. I. Farmer, R. A. Venters, N. R. In Krishna, L. J. Berliner, *Biological Magnetic Resonance*, **1998**, Kluwer/Plenum, New York, pp. 75–120.

[48] D. M. LeMaster, F. M. Richards, *Biochemistry* **1988**, *27*, 142–150.

[49] S. Grzesiek, J. Anglister, A. Bax, J. Anglister, H. Ren, *J. Am. Chem. Soc.* **1993**, *115*, 4369–4370.

[50] J. Fiaux, E. B. Bertelsen, A. L. Horwich, K. Wüthrich, *Nature* **2002**, *418*, 207–211.

[51] S. Rudiger, S. M. V. Freund, D. B. Veprintsev, A. R. Fersht, *Proc. Natl. Acad. Sci. USA* **2002**, *99*, 11085–11090.

[52] R. Sprangers, A. Gribun, P. M. Hwang, W. A. Houry, L. E. Kay, *Proc. Natl. Acad. Sci. USA* **2005**, *102*, 16678–16683.

[53] T. L. Religa, R. Sprangers, L. E. Kay, *Science* **2010**, *328*, 98–102.

[54] R. Sprangers, A. Velyvis, L. E. Kay, *Nat. Methods* **2007**, *4*, 697–703.

[55] C. Huang, P. Rossi, T. Saio, C. G. Kalodimos, *Nature* **2016**, *537*, 202–206.

[56] T. Saio, X. Guan, P. Rossi, A. Economou, C. G. Kalodimos, *Science* **2014**, *344*, 1250494.

[57] K. Lu, Y. Miyazaki, M. F. Summers, *J. Biomol. NMR* **2010**, *46*, 113–125.

[58] L. J. Alvarado, R. M. Leblanc, A. P. Longhini, S. C. Keane, N. Jain, Z. F. Yildiz, B. S. Tolbert, V. M. D'Souza, M. F. Summers, C. Kreutz, T. K. Dayie, *ChemBioChem* **2014**, *15*, 1573–1577.

[59] S. C. Keane, X. Heng, K. Lu, S. Kharytonchyk, V. Ramakrishnan, G. Carter, S. Barton, A. Hosic, A. Florwick, J. Santos, N. C. Bolden, S. McCowin, D. A. Case, B. A. Johnson, M. Salemi, A. Telesnitsky, M. F. Summers, *Science* **2015**, *348*, 917–921.

[60] R. P. Barnwal, E. Loh, K. S. Godin, J. Yip, H. Lavender, C. M. Tang, G. Varani, *Nucleic Acids Res.* **2016**, *44*, 9426–9437.

[61] O. Duss, N. Diarra Dit Konté, F. H. T. Allain, *Methods Enzymol.* **2015**, *565*, 537–562.

[62] A. Marchanka, B. Simon, G. Althoff-Ospelt, T. Carlomagno, *Nat. Commun.* **2015**, *6*, 7024.

[63] E. Karaca, J. P. G. L. M. Rodrigues, A. Graziadei, A. M. J. J. Bonvin, T. Carlomagno, *Nat. Methods* **2017**, *14*, 897–902.

[64] R. Sprangers, L. E. Kay, *Nature* **2007**, *445*, 618–622.

[65] I. Gelis, A. M. J. J. Bonvin, D. Keramisanou, M. Koukaki, G. Gouridis, S. Karamanou, A. Economou, C. G. Kalodimos, *Cell* **2007**, *131*, 756–769.

[66] B. Vögeli, M. Friedmann, D. Leitz, A. Sobol, R. Riek, *J. Magn. Reson.* **2010**, *204*, 290–302.

[67] B. Vögeli, T. F. Segawa, D. Leitz, A. Sobol, A. Choutko, D. Trzesniak, W. Van Gunsteren, R. Riek, *J. Am. Chem. Soc.* **2009**, *131*, 17215–17225.

[68] B. Vögeli, S. Kazemi, P. Güntert, R. Riek, *Nat. Struct. Mol. Biol.* **2012**, *19*, 1053–1058.

[69] B. Vögeli, S. Olsson, P. Güntert, R. Riek, *Biophys. J.* **2016**, *110*, 113–126.

[70] S. Olsson, D. Strotz, B. Vögeli, R. Riek, A. Cavalli, *Structure* **2016**, *24*, 1464–1475.

[71] C. N. Chi, B. Vögeli, S. Bibow, D. Strotz, J. Orts, P. Güntert, R. Riek, *Angew. Chem. Int. Ed.* **2015**, *54*, 11657–11661; *Angew. Chem.* **2015**, *127*, 11823–11827.

[72] B. Vögeli, S. Olsson, R. Riek, P. Güntert, *J. Struct. Biol.* **2015**, *191*, 306–317.

[73] P. Nichols, A. Born, M. Henen, D. Strotz, J. Orts, S. Olsson, P. Güntert, C. Chi, B. Vögeli, *Molecules* **2017**, *22*, 1176.

[74] B. Vögeli, J. Orts, D. Strotz, C. Chi, M. Minges, M. A. Wälti, P. Güntert, R. Riek, *J. Magn. Reson.* **2014**, *241*, 53–59.

[75] B. Fürtig, C. Richter, J. Wöhnert, H. Schwalbe, *ChemBioChem* **2003**, *4*, 936–962.

[76] C. N. Chi, D. Strotz, R. Riek, B. Vögeli, *Chem. Eur. J.* **2018**, *24*, 2270–2276.

[77] P. J. Nichols, M. A. Henen, A. Born, D. Strotz, P. Güntert, B. Vögeli, *Commun. Biol.* **2018**, *1*, 61.

[78] I. Solomon, *Phys. Rev.* **1955**, *99*, 559–565.

[79] A. Kumar, G. Wagner, R. R. Ernst, K. Wüthrich, *J. Am. Chem. Soc.* **1981**, *103*, 3654–3658.

[80] D. Strotz, J. Orts, M. Minges, B. Vögeli, *J. Magn. Reson.* **2015**, *259*, 32–46.

[81] K. Zinovjev, E. Liepinsh, *J. Biophys. Chem.* **2013**, *4*, 58–65.

[82] B. Vögeli, *Prog. Nucl. Magn. Reson. Spectrosc.* **2014**, *78*, 1–46.

[83] B. Vögeli, P. Güntert, R. Riek, *Mol. Phys.* **2013**, *111*, 437–454.

[84] C. N. Chi, D. Strotz, R. Riek, B. Vögeli, *J. Biomol. NMR* **2015**, *62*, 63–69.

[85] F. Delaglio, S. Grzesiek, G. W. Vuister, G. Zhu, J. Pfeifer, A. Bax, *J. Biomol. NMR* **1995**, *6*, 277–293.

[86] D. Strotz, J. Orts, C. N. Chi, R. Riek, B. Vögeli, *J. Chem. Theory Comput.* **2017**, *13*, 4336–4346.

[87] P. Güntert, C. Mumenthaler, K. Wüthrich, *J. Mol. Biol.* **1997**, *273*, 283–298.

[88] P. Güntert, L. Buchner, *J. Biomol. NMR* **2015**, *62*, 453–471.

[89] J. Orts, B. Vögeli, R. Riek, *J. Chem. Theory Comput.* **2012**, *8*, 3483–3492.

[90] J. Lowe, D. Stock, B. Jap, P. Zwickl, W. Baumeister, R. Huber, *Science* **1995**, *268*, 533–539.

[91] A. Förster, E. I. Masters, F. G. Whitby, H. Robinson, C. P. Hill, *Mol. Cell* **2005**, *18*, 589–599.

[92] V. Tugarinov, R. Sprangers, L. E. Kay, *J. Am. Chem. Soc.* **2007**, *129*, 1743–1750.

[93] S. Nozinovic, B. Fürtig, H. R. A. Jonker, C. Richter, H. Schwalbe, *Nucleic Acids Res.* **2010**, *38*, 683–694.

[94] M. H. Bailor, C. Musselman, A. L. Hansen, K. Gulati, D. J. Patel, H. M. Al-Hashimi, *Nat. Protoc.* **2007**, *2*, 1536–1546.

[95] I. C. Felli, C. Richter, C. Griesinger, H. Schwalbe, *J. Am. Chem. Soc.* **1999**, *121*, 1956–1957.

[96] H. Schwalbe, T. Carlomagno, M. Hennig, J. Junker, B. Reif, C. Richter, C. Griesinger, *Methods Enzymol.* **2002**, *338*, 35–81.

[97] J. Boisbouvier, B. Brutscher, A. Pardi, D. Marion, J. P. Simorre, *J. Am. Chem. Soc.* **2000**, *122*, 6779–6780.

[98] C. M. Grytz, S. Kazemi, A. Marko, P. Cekan, P. Güntert, S. T. Sigurdsson, T. F. F. Prisner, *Phys. Chem. Chem. Phys.* **2017**, *19*, 29801–29811.

[99] J. Ferner, A. Villa, E. Duchardt, E. Widjajakusuma, J. Wöhnert, G. Stock, H. Schwalbe, *Nucleic Acids Res.* **2008**, *36*, 1928–1940.

[100] P. Vallurupalli, L. E. Kay, *J. Am. Chem. Soc.* **2005**, *127*, 6893–6901.

[101] J. Rinnenthal, C. Richter, S. Nozinovic, B. Fürtig, J. J. Lopez, C. Glaubitz, H. Schwalbe, *J. Biomol. NMR* **2009**, *45*, 143–155.

[102] G. M. Giambaşu, D. M. York, D. A. Case, *RNA* **2015**, *21*, 963–974.